ELSEVIER

Journal of Nuclear Materials 266–269 (1999) 993–996

journal of nuclear materials

Turbulence in boundary plasmas

X.Q. Xu [a,*], R.H. Cohen [a], G.D. Porter [a], J.R. Myra [b], D.A. D'Ippolito [b], R. Moyer [c]

[a] *Lawrence Livermore National Laboratory, University of California, Livermore, CA 94550, USA*
[b] *Lodestar Research Corporation, Boulder, CO 80301, USA*
[c] *University of California, San Diego, La jolla, CA 92093, USA*

Abstract

We simulate boundary plasma turbulence using a 3D turbulence code BOUT and a linearized electromagnetic instability shooting code BAL. The code BOUT solves fluid equations for plasma vorticity, density, ion temperature and parallel momentum (along the magnetic field), electron temperature, and parallel momentum. A realistic DIII-D X-point magnetic geometry is used. The focus is on the possible local linear instability drives and turbulence suppression mechanisms involved in the L–H transition and on the consistency of the computed turbulence with observed temperature and density profiles. Comparison is made with data from the DIII-D tokamak where probe measurements provide turbulence statistics in the boundary plasma and transport modeling.

Keywords: DIII-D; Divertor plasma; Langmuir probe

1. Introduction

Turbulence in the plasma boundary of tokamaks is of concern due to its importance in governing the ability to achieve enhanced confinement modes in the core as well as transport (and thus divertor heat loads) in the scrape-off layer (SOL) plasma. Specifically, the boundary turbulence determines how the $E \times B$ shear layer is generated and how the transport barrier is formed. The unstable normal modes in the plasma boundary region have a different character than in the core due to low temperature, steep gradients of plasma profiles, and the X-point divertor geometry.

In an effort to better understand the turbulence dynamics, we simulate the boundary plasma for the DIII-D tokamak using the 3D global turbulence code BOUT [1] and a linearized electromagnetic instability shooting code BAL [2]. Our primary focus here is on the possible local linear instability drives, turbulence saturation levels and comparison of power spectra with probe measurements. In Section 2, we give our reduced set of dynamical equations in our simulation, and the simulation model is described in Section 3. Section 4 contains a comparison between the experiment and the simulation including discussion of the importance of assumptions in the model, and we give a summary in Section 5.

2. Dynamic equations

In the boundary plasma, the application of a fluid model is reasonable in part because of the low temperature and high collisionality. Further, the dominant modes in our simulations are in the long wavelength regimes, $k_\perp \rho_s \ll 1$ at separatrix, consistent with a fluid approach. Thus an appropriate set of equations to describe the turbulence is given by a six-field model obtained by reduction of the Braginskii Equations [3]:

$$\frac{\partial j_\|}{\partial t} + \nabla \cdot (U j_\|) = \frac{ne^2}{m_e}\left(\nabla_\| n + 1.71\nabla_\| T_e + E_\| + \frac{v_e \times B \cdot b_0}{e}\right)$$

* Corresponding author. Tel.: +1 510 423 7578; fax: +1 510 423 3484; e-mail: xxu@llnl.gov

PII: S 0 0 2 2 - 3 1 1 5 (9 8) 0 0 6 2 7 - 8

$$
\begin{aligned}
&-\nu_{ei}j_{\|} + \frac{ne^2}{m_e}\left(\tilde{b}\cdot\nabla n + 1.71\tilde{b}\cdot\nabla T_e + \tilde{b}\cdot\nabla\phi\right)\\
&+ 0.46\chi^c_{\|e}\nabla_{\|}\left(T_e^{5/2}\nabla_{\|}(j_{\|}/ne + V_i)\right), \qquad (1)
\end{aligned}
$$

$$
\begin{aligned}
&\frac{\partial\varpi}{\partial t} + \nabla\cdot[(U+V_i)\varpi] = \left(\frac{nce}{\omega_{ci}B}\right)^{-1} 2\frac{b_0\times\kappa\cdot\nabla P}{n}\\
&+ \left(\frac{nce}{\omega_{ci}B}\right)^{-1}\nabla_{\|}j_{\|} + \left(\frac{nce}{\omega_{ci}B}\right)^{-1}\mu_{ii}\nabla_{\perp}^2\varpi, \qquad (2)
\end{aligned}
$$

$$
\begin{aligned}
&\frac{\partial n}{\partial t} + \nabla\cdot[(U+V_i)n] = 2b_0\times\kappa\cdot\nabla(P_e-\phi)\\
&+ \nabla_{\|}\left(\frac{j_{\|}}{e} - nV_i\right), \qquad (3)
\end{aligned}
$$

$$
\begin{aligned}
&\frac{\partial T_i}{\partial t} + \nabla\cdot[(U+V_i)T_i] = \frac{4}{3}b_0\times\kappa\cdot\nabla(P_e-\phi)\\
&+\frac{2}{3}\chi^c_{\|i}\nabla_{\|}\left(T_i^{5/2}\nabla_{\|}T_i\right) - \frac{2T_i}{3}\left(\nabla_{\|}V_i - \frac{1}{n}\nabla_{\|}j_{\|}\right)\\
&+\frac{2}{3n}\left(\frac{16}{3\tau}\mu_{ii}\right)\nabla_{\perp}^2 T_i, \qquad (4)
\end{aligned}
$$

$$
\begin{aligned}
&\frac{\partial T_e}{\partial t} + \nabla\cdot(UT_e) = \frac{4}{3}b_0\times\kappa\cdot\nabla(P_e-\phi)\\
&+\frac{2}{3}\chi^c_{\|e}\nabla_{\|}\left(T_e^{5/2}\nabla_{\|}T_e\right) - \frac{2T_e j_{\|}}{3n^2}\tilde{b}\cdot\nabla N_0 - \frac{2T_e}{3}\left(\nabla_{\|}V_i\right.\\
&\left.-\frac{1.71}{n}\nabla_{\|}j_{\|} + \frac{j_{\|}}{n^2}\nabla_{\|}n\right), \qquad (5)
\end{aligned}
$$

$$
\begin{aligned}
&\frac{\partial V_i}{\partial t} + \nabla\cdot[(U+V_i)V_i]\\
&= -\frac{1}{nM_i}\nabla_{\|}P - \frac{1}{nM_i}\tilde{b}\cdot\nabla P_0 + \mu_{\|}\nabla_{\|}^2 V_i, \qquad (6)
\end{aligned}
$$

where $U = cb_0\times\nabla_{\perp}\phi/B$, $E_{\|} = -\nabla_{\|}\phi - (1/c)\partial A_{\|}/\partial t$, $\nabla_{\perp}\cdot[b_0\times(v_{E\times B}+v_{Pi})B/c] = -\varpi$, $\nabla_{\perp}^2 A_{\|} = -(4\pi/c)j_{\|}$, $\nabla_{\|} = \nabla_{\|}^0 + \tilde{b}\cdot\nabla$, $\tilde{b} = \tilde{B}/B$, $\nabla_{\|}^0 = b_0\cdot\nabla$, $\kappa = b_0\cdot\nabla b_0$. ν_{ii}, $\mu_{\|}$, $\chi^c_{\|}$ are the classical diffusion coefficients, and ν_{ei} is electron collision frequency. Except for the ion temperature equation and parallel electron viscous damping, the equations were described in Ref. [1]. The parallel electron viscous damping is necessary to smooth the high $k_{\|}$ oscillations near the X-point region. The ion temperature equation appears to be important for the turbulence-generated electric fields via the ion diamagnetic drift and possibly introduces the η_i-mode in the inner edge region.

3. Numerical model

In order to efficiently simulate turbulence with short perpendicular wavelength $k_{\|} \ll k_{\perp}$ we choose field-line-aligned ballooning coordinates, x, y and z, which are related to the usual flux coordinates ψ, θ, and φ by the relation $x = \psi - \psi_s, y = \theta, z = \varphi - \int q(x,y)\,\mathrm{d}y$. The

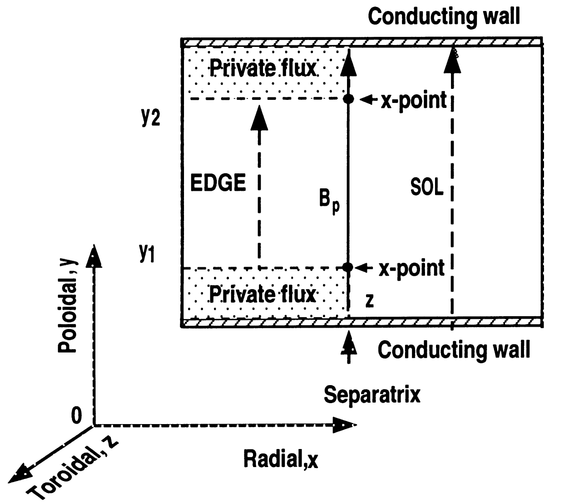

Fig. 1. 2D Plan showing the regions used in 3D simulation code BOUT.

partial derivatives are: $\mathrm{d}/\mathrm{d}\psi = \partial/\partial x - (\int \partial q/\partial\psi)\partial/\partial z$, $\mathrm{d}/\mathrm{d}\theta = \partial/\partial y - q\partial/\partial z, \mathrm{d}/\mathrm{d}\varphi = \partial/\partial z$, and $\nabla_{\|} = (B_p/hB)\partial/\partial y$. The magnetic separatrix is denoted by $\psi = \psi_s$. Here the key ballooning assumption is $|\partial/\partial y| \ll |q\partial/\partial z|$ and $\mathrm{d}/\mathrm{d}\theta \simeq -q\partial/\partial z$. In this choice of coordinates, y, the poloidal angle, is also the coordinate along the field line. The radial-poloidal plane is given in Fig. 1. The mesh in this plane uses as one coordinate the poloidal magnetic flux surfaces as constructed by the EFIT code. With poloidal flux, ψ, normalized to unity on the separatrix, we typically take the inner simulation boundary condition to be $\psi_c = 0.95$ and the outer boundary at $\psi_w = 1.05$. The boundary conditions is homogeneous Neumann at $x = x_c$ and Dirichlet at $x = x_w$, sheath boundaries in y in the SOL and the private flux regions, periodic in y in "edge" (inside of separatrix), and periodic in z.

The BOUT code solves for the plasma fluid equations in a 3-D toroidal segment, including the region somewhat inside the separatrix and extending into the SOL. A finite difference method is used, and the resulting difference equations are solved with a fully implicit Newton–Krylov solver CVODE/PVODE [4,5].

4. Simulation of the boundary turbulence and comparison with the experiment

Our first application of BOUT is to study pedestal physics and the L–H transition. We focus on the analysis of discharge 89840 of DIII-D in the boundary plasma. This discharge was selected because it is one of a series taken to document the behavior of the plasma during a slow L- to H-mode transition. There are mid-plane reciprocating probe measurements for the L- and H-mode plasma on this discharge [6]. In order to investigate pedestal physics, we first run the edge plasma transport code UEDGE/EFIT to get the magnetic geometry for this discharge in L and H mode. We then obtain equilibrium plasma profiles by using hyperbolic tangent fits to the experimental data for plasma density N_{i0}, electron temperature T_{e0}, ion temperature T_{i0} [7]. We find that there is little change in the magnetic geometry in L and H mode. The plasma density N_{i0} is steepened by a factor of 4 and the electron temperature is steepened by a factor of 1.5 from L to H mode. Since there is no ion temperature measurement for L mode we assume $T_{i0} = T_{e0}$.

In Eqs. (1)–(6), there are many local instability drives as discussed in Ref. [1]. Given the above plasma parameters, two separate dominant modes are found by running BAL and BOUT. (1) In the absence of $E \times B$ shearing, an ideal MHD type mode is found in H-mode in the edge with low toroidal mode number n, extending up to $n = 60$. This is a possible candidate for the coherent mode found in DIII-D in H-mode [8]. The effect of shearing on the mode is under investigation. (2) A broad-band high-n mode is found, peaked around $n = 220$, both for L mode and H mode. The details of the linear instability analysis and simulations will be given in a future publication.

We have run a number of simulations using the electrostatic version of BOUT under L-mode and H-mode plasma conditions. The qualitative ballooning mode structure is similar to Fig. 2(b) and (c) in Ref. [1]. The frequency spectra of the mid-plane particle flux from probe measurements and BOUT simulations in L mode in Fig. 2 shows reasonable agreement; there is a two-scale fall off in the spectrum, $1/f$ scaling at low frequency and $1/f^4$ scaling at high frequency separated around 200 MHz. The radial profiles of the ensemble averaged turbulence diffusion coefficient $\chi_i(x)$ and turbulence generated electric field $E_x(x)$ are shown in Figs. 3 and 4. We find (1) spatial profiles of the turbulence-generated diffusivity in qualitative agreement with those required to yield pedestal plasma profiles in plasma boundary; (2) turbulence-generated electric field profiles across the separatrix qualitatively consistent with H-mode experiments. As is shown in Fig. 3, the turbulence-generated diffusivity is larger in flat regions (top of pedestal) and small in the steep gradient region

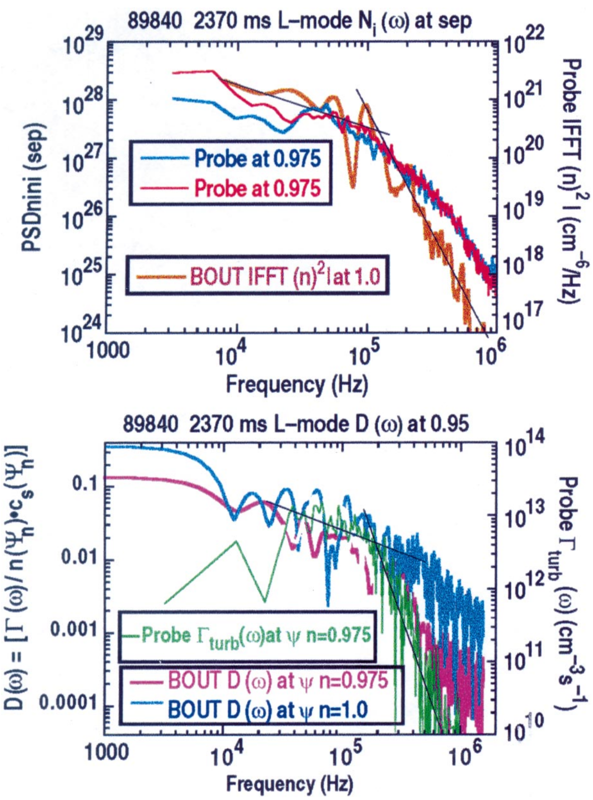

Fig. 2. Comparison of power spectra from Probe data and BOUT L-mode simulations. Shots 89840 at $t = 2370$ ms (BOUT) and shots 89835 and 89842 (probe).

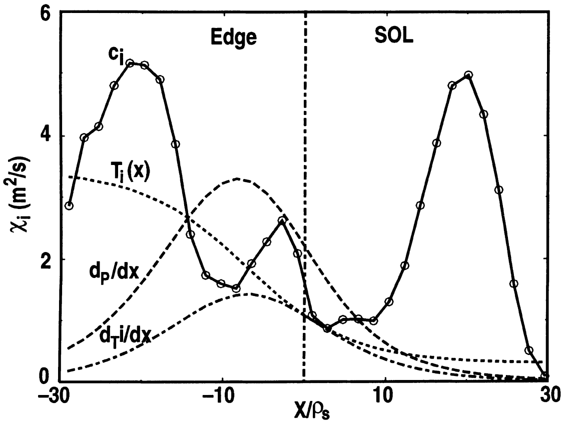

Fig. 3. Turbulence-generated heat diffusivity χ_i in L mode from BOUT simulations. The solid line is the computed χ_i; the dotted line is the equilibrium ion temperature profile $T_i(x)$, the dashed line is the inverse-radial-gradient scale length ρ_s/L_P of total pressure P normalized to the separatrix value, and the dot-dashed line is the inverse-radial-gradient scale length ρ_s/L_{Ti} of ion temperature normalized to the separatrix value.

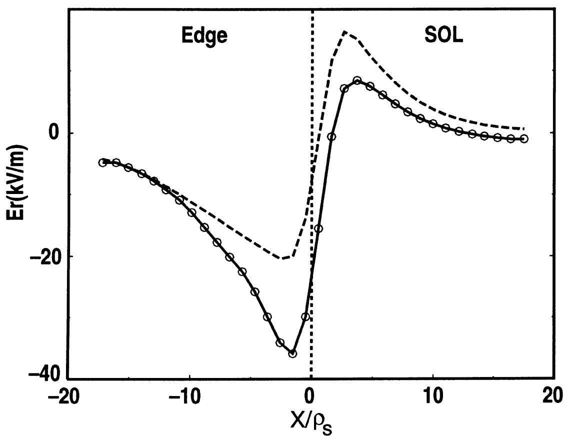

Fig. 4. Electric field $E_x(x)$ in H mode from BOUT simulations. The solid line is the computed $E_x(x)$ including the turbulence-generated contribution, the dashed line is the equilibrium electric field calculated from the smoothed diamagnetic flow and the sheath potential in the SOL.

(pedestal edge). These are necessary conditions to form the pedestal plasma profiles. The non-monotonic radial dependence of the turbulence-generated diffusivity is under investigation. We have also run the case by turning off the electric field, and find that the SOL transport is reduced due to finite polarization stabilization of SOL modes [9].

5. Summary

We have investigated boundary plasma turbulence in L and H mode using the BOUT turbulence code and the BAL linearized shooting code. We have found broad-band toroidal-mode-number turbulence peaked around $n = 220$, dominated by the combination of bad curvature and steep radial gradients. The BOUT simulations and probe measurements show similar frequency spectra for the mid-plane particle flux. The reduction of particle flux from L to H mode is also consistent with the results in experimental modeling [7].

These simulations show the feasibility of modeling some aspects of L to H transition with the turbulence code BOUT; the detailed dynamics of L to H transition requires the evolution of background plasma profiles. Important additional work to be done is to include sources and sinks in BOUT and to evolve the plasma profile self-consistently or to dynamically couple the BOUT to an edge transport code such as UEDGE.

Acknowledgements

We gratefully acknowledge discussions with A.C. Hindmarsh, Lynda LoDestro, Nathan Mattor, T.D. Rognlien, and Dimitri Ryutov. This work was performed under the auspices of the US Department of Energy by Lawrence Livermore National Laboratory under Contract No. W-7405-Eng-48, and Grants DE-FG03-97ER54392 at Lodestar Research and DE-FG03-95ER54294 at UCSD.

References

[1] X.Q. Xu, R.H. Cohen, Contrib. Plasma Phys. 36 (1998) 158.
[2] J.R. Myra, D.A. D'Ippolito, J.P. Goedbloed, Phys. Plasmas 4 (1997) 1330.
[3] S.I. Braginskii, in: M.A. Leontovich (Ed.), Transport processes in a plasma, Reviews of Plasma Physics, vol. 1, Consultants Bureau, New York, 1965, p. 205.
[4] S.D. Cohen, A.C. Hindmarsh, Comp. in Phys. 10 (1996) 138; M.R. Wittman, Lawrence Livermore National Laboratory Report No. UCRL-ID-125562, 1996.
[5] A.C. Hindmarsh, Lawrence Livermore National Laboratory Report No. UCRL-TB-125577, Rev. 1, 1997.
[6] R. Moyer et al., these Proceedings.
[7] G.D. Porter et al., hTupP2 15, APS conference, Div. Plasma Phys., Pittsburgh, PA, 1997.
[8] R. Moyer et al., hTupP2 32, APS conference, Div. Plasma Phys., Pittsburgh, PA, 1997.
[9] R.H. Cohen, X.Q. Xu, Phys. Plasmas 2 (1995) 3374.